Simultaneous optimization of gait and design parameters for bipedal robots

Ulrich J. Römer[1], Cornelius Kuhs[2], Mathias J. Krause[3] and Alexander Fidlin[1]

Abstract— A walking bipedal robot's energy efficiency depends on its gait as well as its design, whereas design changes affect the optimal gaits. We propose a method to take these interdependencies into account via simultaneous optimization of gait as well as design parameters. The method is applied to a planar robot with hybrid zero dynamics control and a torsion spring between its thighs. Periodic gaits are simulated by means of the hybrid zero dynamics. The implementation of the simultaneous optimization of gait parameters and spring stiffness via sequential quadratic programming is presented. Subsequently, an error analysis is performed to gain good convergence and short computation times of the optimization. The evaluation of gradients is identified as crucial for the algorithm's convergence and therefore performed via complex step derivative approximations. The resulting implementation exhibits good convergence behavior and is provided as supplement to this paper. At 2.3 m/s, the simultaneous optimization results in savings in energy expenditure of up to 55%. A consecutive optimization of first gait and then stiffness yields only 11%, demonstrating the advantage of the presented method.

I. INTRODUCTION

Besides stable control, energy efficiency is a major objective in robotics in general and (autonomous) bipedal robots in particular. The generation of optimal gaits is thus an ongoing object of research [1]–[15]. The basis of optimal gait generation is numerical optimization which is performed either in offline simulations [6] or within real-time optimal control [15], [16]. Different objectives have been proposed as criterion for optimality [9], [10], many of which relate to energy efficiency.

Among the control strategies for bipedal robots, some of the most widely used approaches are designing walking controllers around the zero moment point (ZMP) [17] and the concept of capture point control [18]. These approaches, however, focus mainly on stabilization, not on energy efficiency. Another approach is hybrid zero dynamics (HZD) based control [13], [14], [19], [20] which stabilizes the system around predefined reference trajectories and was successfully implemented on several platforms such as RABBIT [21], ERNIE [22] and MABEL [23]. These robots typically posses few degrees of freedom and one degree of underactuation [13], [21]–[23], although extensions of the

models' complexity [14], [20] as well as the incorporation of full and overactuated phases have been proposed [19]. The system's natural dynamics can evolve due to the underactuation. Energy efficient gaits can be generated via offline optimization of the reference trajectories [1], [2], [10], [13].

However, energy efficient locomotion does not only depend on the robot's gait but also on its parameters (e.g. mass distribution, dimensions, stiffnesses). Changes of design parameters affect the optimal gaits and considerably influence efficiency [1], [2], [12], [24]. While some parameters like stiffnesses [25] may be adjusted after assembly, most parameters are fixed. A method which can be used during the design of a robot to increase energy efficiency as well as to identify the most critical parameters is simultaneous optimization of gait and design parameters via numerical simulations. In [1], [2], a bilevel optimization of the robot's parameters (stiffnesses) via a gradient-free upper-level method in combination with a gradient-based lower-level for optimal gait generation is proposed. The upper-level optimizes the average energy efficiency of several gaits in a speed range to counteract specialization for one specific speed. The drawbacks of this approach are long computation times due to the gradient-free upper-level optimization. However, it is necessary since convergence could not be achieved with a gradient-based algorithm.

The aim of this paper is to develop a gradient-based, single-level method based on sequential quadratic programming (SQP) for simultaneous gait and design parameter optimization with good convergence and short computation times. To achieve these objectives, we present an error analysis for the implementation which focuses on the numeric evaluation of integrals and gradients. The remainder of this paper is structured as follows: A planar robot with a torsion spring between its thighs and HZD control is modeled in Sec. II. The objective, the constraints as well as the implementation of the simultaneous optimization are presented in Sec. III. Sec. IV shows an investigation of the numerical evaluation and implementation with focus on error propagation and convergence. The computation of gradients is identified to be crucial and therefore performed via complex step derivative approximations [26], [27]. Sec. V presents the results for the simultaneous optimization of the spring stiffness and one gait (2.3 m/s) as well as several gaits (speed range: 0.3-2.3 m/s) to reduce the specialization inherent to optimization. The advantage of the proposed method is illustrated via comparisons to consecutive optimizations where either the gait is optimized for fixed stiffness, or vice versa. A conclusion is given in Sec. VI.

[1]Ulrich Römer and Alexander Fidlin are with Institute of Engineering Mechanics (ITM), Karlsruhe Institute of Technology
`ulrich.roemer@kit.edu`
`alexander.fidlin@kit.edu`
[2]Cornelius Kuhs is a student at Karlsruhe Institute of Technology
[3]Mathias J. Krause is with Institutes for Mechanical Process Engineering and Mechanics (IMVM) and Applied and Numerical Mathematics (IANM), Karlsruhe Institute of Technology, 76131 Karlsruhe, Germany
`mathias.krause@kit.edu`

II. ROBOT MODEL

The robot model for subsequent optimization is depicted in Fig. 1. The planar multibody system consists of a rigid upper body (index HAT: **h**ead, **a**rms, **t**orso), two thighs and two shanks which are connected by actuated, ideal revolute joints in the hip and knees. The robot's point feet do not allow for any torque transmission between the legs and the ground, thereby resulting in one degree of underactuation. The contact between the stance leg and the ground is therefore modeled as an unactuated revolute joint with the constraints of unilaterality (no lift-off) and stiction (no slipping). This model, which is frequently used for HZD control [13], [21]–[23], is extended by coupling the robot's thighs via a linear torsion spring with stiffness k in the hip.

Periodic bipedal walking is modeled as an alternating series of single support (SSP) (Sec. II-A) and instantaneous double support phases (impacts) (Sec. II-B) resulting in a hybrid system[1]. A trajectory tracking feedback controller (Sec. II-C) is added to produce stable walking gaits. Consideration of the model's symmetry as well as the motion's periodicity in the design of the reference trajectories allows for an efficient calculation of the corresponding gait. The controlled system's hybrid zero dynamics – the remaining, uncontrollable dynamics with perfect trajectory tracking – resembles a mechanical model with one degree of freedom. A solution of this dynamics for periodic walking can be computed in closed form. The corresponding actuator torques for subsequent optimization are obtained via inverse dynamics.

A. Single support model

The SSP is described by the equation of motion

$$\begin{bmatrix} M_{s,11} & \mathbf{M}_{s,12} \\ \mathbf{M}_{s,21} & \mathbf{M}_{s,22} \end{bmatrix} \begin{bmatrix} \ddot{\theta} \\ \ddot{\mathbf{q}}_b \end{bmatrix} + \begin{bmatrix} \Gamma_{s,1} \\ \mathbf{\Gamma}_{s,2} \end{bmatrix} = \begin{bmatrix} \mathbf{B}_{s,1} \\ \mathbf{B}_{s,2} \end{bmatrix} \mathbf{u} \qquad (1)$$

of the stance model (index: s) in Fig. 1a with the body coordinates $\mathbf{q}_b = [\theta_{H1}\ \theta_{H2}\ \theta_{K1}\ \theta_{K2}]^T$, the SSP coordinates $\mathbf{q}_s = [\theta\ \mathbf{q}_b^T]^T$, the mass matrix $\mathbf{M}_s(\mathbf{q}_b)$, the generalized forces $\mathbf{\Gamma}_s(\mathbf{q}_s, \dot{\mathbf{q}}_s)$ (gravity and Coriolis forces), the input matrix $\mathbf{B}_s$ ($\mathbf{B}_{s,1} = \mathbf{0}$: zero matrix; $\mathbf{B}_{s,2} = \mathbf{I}$: identity matrix) and the input vector $\mathbf{u}$. The absolute orientation of the robot is described by the angle θ which increases monotonically during one step and is thus used to parameterize the controller's reference trajectories in Sec. II-C.

The system's inputs $\mathbf{u} = \mathbf{u}_M + \mathbf{u}_S$ are the joint torques in hip and knees corresponding to the body coordinates $\mathbf{q}_b$. They consist of actuator (motor) torques $\mathbf{u}_M$ and spring torques

$$\mathbf{u}_S = \begin{bmatrix} \mathbf{K} & \mathbf{0} \\ \mathbf{0} & \mathbf{0} \end{bmatrix} \mathbf{q}_b , \quad \mathbf{K} = \begin{bmatrix} -k & k \\ k & -k \end{bmatrix} . \qquad (2)$$

The inverse dynamics for the joint torques result from the solution of the first row of (1) for $\ddot{\theta}$ and subsequent

[1]The time continuous SSP is described by a differential equation, the impacts are modeled via discrete mappings.
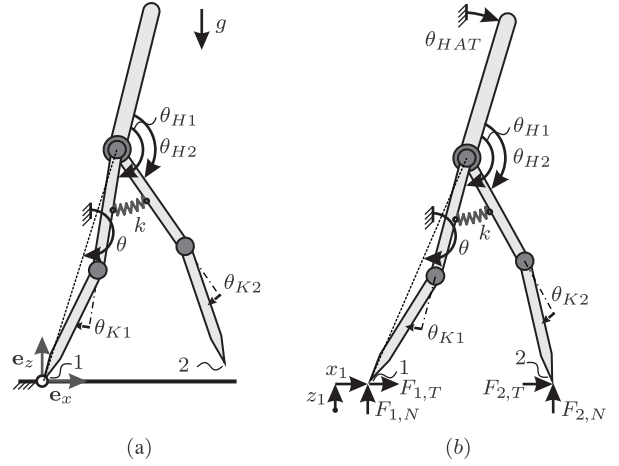

Fig. 1. Constrained robot model (a) for single support phase and free robot model (b) for derivation of ground contact forces.

substitution of the result into the second row

$$\mathbf{u} = \left(\mathbf{M}_{s,22} - \mathbf{M}_{s,21} M_{s,11}^{-1} \mathbf{M}_{s,12} \right) \ddot{\mathbf{q}}_b$$
$$+ \left(\mathbf{\Gamma}_{s,2} - \mathbf{M}_{s,21} M_{s,11}^{-1} \Gamma_{s,1} \right) . \qquad (3)$$

The ground contact force, which is required to verify the assumptions of unilaterality and stiction, is derived from the free model (index: f) in Fig. 1b. The generalized coordinates of the free model are $\mathbf{q}_f = [\mathbf{r}_1^T\ \mathbf{q}_s^T]^T$ with the stance foot position $\mathbf{r}_1 = [x_1\ z_1]^T$. The free model's equation of motion is

$$\begin{bmatrix} \mathbf{M}_{f,00} & \mathbf{M}_{f,01} \\ \mathbf{M}_{f,10} & \mathbf{M}_{f,11} \end{bmatrix} \begin{bmatrix} \ddot{\mathbf{r}}_1 \\ \ddot{\mathbf{q}}_s \end{bmatrix} + \begin{bmatrix} \mathbf{\Gamma}_{f,0} \\ \mathbf{\Gamma}_{f,1} \end{bmatrix} = \begin{bmatrix} \mathbf{0} \\ \mathbf{B}_s \end{bmatrix} \mathbf{u} + \left(\frac{\partial \mathbf{r}_1}{\partial \mathbf{q}_f} \right)^T \mathbf{F}_1 \qquad (4)$$

with mass matrix $\mathbf{M}_f(\mathbf{q}_f)$, generalized forces $\mathbf{\Gamma}_f(\mathbf{q}_f, \dot{\mathbf{q}}_f)$, ground contact force $\mathbf{F}_1 = [F_{1,x}\ F_{1,z}]^T$ and the projection matrix $(\partial \mathbf{r}_1 / \partial \mathbf{q}_f)$ which can be derived with the virtual work principle. The swing foot is not in contact with the ground during the SSP, therefore $\mathbf{F}_2 = [F_{2,x}\ F_{2,z}]^T = \mathbf{0}$.

Substitution of the relation $(\partial \mathbf{r}_1 / \partial \mathbf{q}_f)^T \mathbf{F}_1 = \begin{bmatrix} \mathbf{F}_1^T & \mathbf{0} \end{bmatrix}^T$ and the constraints $\mathbf{r}_1 = \dot{\mathbf{r}}_1 = \ddot{\mathbf{r}}_1 = \mathbf{0}$ into the first row of (4) results in the ground contact force

$$\mathbf{F}_1 = \mathbf{M}_{f,01}(\mathbf{q}_s)\ \ddot{\mathbf{q}}_s + \mathbf{\Gamma}_{f,0}(\mathbf{q}_s, \dot{\mathbf{q}}_s) . \qquad (5)$$

B. Impact model

The double support phase is modeled as plastic impact (no rebound, no slipping) of the free model's swing foot on the ground. The assumption of an instantaneous impact allows for the derivation of an algebraic mapping of the robot's state directly before (index: $-$) to its state after the impact ($+$) [28]. The legs' roles are switched after the impact (the former stance leg becomes the new swing leg and vice versa) which is incorporated into the mapping. The absolute orientation is described via θ_{HAT} (c.f. Fig. 1b) which is independent of the legs' roles and allows for a clear formulation of the impact maps in Sec. II-C. Therefore, the transformation $\mathbf{\Psi}$ from $\hat{\mathbf{q}}_s = \begin{bmatrix} \theta_{HAT} & \mathbf{q}_b^T \end{bmatrix}^T$ to

$$\mathbf{q}_s = \mathbf{\Psi}(\hat{\mathbf{q}}_s) \qquad (6)$$

as well as its Jacobian

$$\frac{\partial \mathbf{\Psi}}{\partial \hat{\mathbf{q}}_s} =: \mathbf{J}_\Psi = \begin{bmatrix} \mathbf{J}_{\Psi,1} \\ \mathbf{J}_{\Psi,2} \end{bmatrix} = \begin{bmatrix} \partial\theta/\partial\hat{\mathbf{q}}_s \\ \partial\mathbf{q}_b/\partial\hat{\mathbf{q}}_s \end{bmatrix} \quad (7)$$

are defined. In order to derive the impact mapping, the equation of motion of the free model with the coordinates $\hat{\mathbf{q}}_f = [\mathbf{r}_1^T \, \hat{\mathbf{q}}_s^T]^T$ is derived analogously to (4) and integrated over the infinitesimal impact duration

$$\hat{\mathbf{M}}_f(\hat{\mathbf{q}}_f^+)\,\dot{\hat{\mathbf{q}}}_f^+ - \hat{\mathbf{M}}_f(\hat{\mathbf{q}}_f^-)\,\dot{\hat{\mathbf{q}}}_f^- = \lim_{t^- \to t^+} \int_{t^-}^{t^+} \left(\frac{\partial\mathbf{r}_2}{\partial\hat{\mathbf{q}}_f} \right)^T \mathbf{F}_2 \, \mathrm{d}t$$
$$=: \left(\frac{\partial\mathbf{r}_2}{\partial\hat{\mathbf{q}}_f} \right)^T \hat{\mathbf{F}}_2 \ . \quad (8)$$

The stance foot is assumed to lift off without interaction, therefore $\mathbf{F}_1 = \mathbf{0}$ subject to the condition $\dot{z}_1^+ > 0$. The free model's mass matrix[2] is $\hat{\mathbf{M}}_f(\hat{\mathbf{q}}_f)$ and the position vector of the impacting foot is $\mathbf{r}_2 = [x_2 \, z_2]^T$. The robot's configuration $\hat{\mathbf{q}}_f = \hat{\mathbf{q}}_f^+ = \hat{\mathbf{q}}_f^-$ does not change during the impact. With the plastic impact condition

$$\dot{\mathbf{r}}_2^+ = \frac{\partial\mathbf{r}_2}{\partial\hat{\mathbf{q}}_f}\,\dot{\hat{\mathbf{q}}}_f^+ = \mathbf{0} \ , \quad (9)$$

a system of linear equations

$$\begin{bmatrix} \hat{\mathbf{M}}_f & -\frac{\partial\mathbf{r}_2}{\partial\hat{\mathbf{q}}_f}^T \\ \frac{\partial\mathbf{r}_2}{\partial\hat{\mathbf{q}}_f} & \mathbf{0} \end{bmatrix} \begin{bmatrix} \dot{\hat{\mathbf{q}}}_f^+ \\ \hat{\mathbf{F}}_2 \end{bmatrix} = \begin{bmatrix} \hat{\mathbf{M}}_f \\ \mathbf{0} \end{bmatrix} \dot{\hat{\mathbf{q}}}_f^- \quad (10)$$

can be formulated. To account for the legs' change of role, an impact map (relabeling matrix) $\mathbf{\Delta}_q$ for the angles is introduced, so that

$$\hat{\mathbf{q}}_s^+ = \mathbf{\Delta}_q \, \hat{\mathbf{q}}_s^- \ . \quad (11)$$

Equation (10) can be solved symbolically using a computer algebra system and results in two impact maps for the velocities and impact forces

$$\dot{\hat{\mathbf{q}}}_s^+ = \mathbf{\Delta}_{\dot{q}} \, \dot{\hat{\mathbf{q}}}_s^- \ , \quad (12)$$
$$\hat{\mathbf{F}}_2 = \mathbf{\Delta}_F \, \dot{\hat{\mathbf{q}}}_s^- \ . \quad (13)$$

C. Control model

A trajectory tracking feedback controller which generates stable periodic walking gaits can be designed by using input-output linearization[3] [13], [14]. Due to the underactuation, the controlled system's hybrid zero dynamics resembles a mechanical model with one degree of freedom (the absolute orientation). Autonomous HZD are obtained via the introduction of state dependent, rather than time dependent, reference trajectories. The trajectories' parameterization is designed to implicitly satisfy the periodicity conditions at the beginning/end of a step which is necessary a condition for the controller's stability [14]. Thereby, the solution of one step defines the gait completely. The remaining HZD differential equation is transformed to a time-free, scalar equation which can be solved in closed form via quadrature.

[2]$\hat{\mathbf{M}}_f$ results from a canonical transformation of $\mathbf{M}_f$ using $\mathbf{\Psi}$.
[3]This section is a compressed summary of the HZD. For a detailed derivation of the controller refer to [14].

Another quadrature yields the solution for the corresponding time. The angular velocities and actuator torques can be computed from algebraic equations based on those solutions.

The reference trajectories for the body coordinates $\mathbf{q}_b$ during the SSP are defined via Bézier polynomials in θ of degree M

$$\mathbf{q}_b(\boldsymbol{\alpha}, \theta) = \sum_{k=0}^M \boldsymbol{\alpha}_k \frac{M!}{k!(M-k)!} s^k (1-s)^{M-k} \ , \quad (14)$$
$$s = \left(\frac{\theta - \theta^+}{\theta^- - \theta^+} \right)$$

with the Bézier parameters $\boldsymbol{\alpha} = [\boldsymbol{\alpha}_0 \, \boldsymbol{\alpha}_1 \ldots \boldsymbol{\alpha}_M]$ and θ^+, θ^-. The reference velocities and accelerations are

$$\dot{\mathbf{q}}_b(\boldsymbol{\alpha}, \theta, \dot\theta) = \frac{\partial\mathbf{q}_b}{\partial\theta} \dot\theta \ , \quad (15)$$
$$\ddot{\mathbf{q}}_b(\boldsymbol{\alpha}, \theta, \dot\theta, \ddot\theta) = \frac{\partial^2\mathbf{q}_b}{\partial\theta^2} \dot\theta^2 + \frac{\partial\mathbf{q}_b}{\partial\theta} \ddot\theta \ ; \quad (16)$$

the reference states before and after the impact

$$\mathbf{q}_b^+ = \boldsymbol{\alpha}_0 \ , \quad \dot{\mathbf{q}}_b^+ = \frac{M}{\theta^- - \theta^+}(\boldsymbol{\alpha}_1 - \boldsymbol{\alpha}_0)\,\dot\theta^+ \ , \quad (17)$$
$$\mathbf{q}_b^- = \boldsymbol{\alpha}_M \ , \quad \dot{\mathbf{q}}_b^- = \frac{M}{\theta^- - \theta^+}(\boldsymbol{\alpha}_M - \boldsymbol{\alpha}_{M-1})\,\dot\theta^- \ . \quad (18)$$

To incorporate the periodicity conditions into the reference trajectories, the parameters $\boldsymbol{\alpha}_0$, $\boldsymbol{\alpha}_1$, θ^+ and θ^- are expressed as functions of $\boldsymbol{\alpha}_{2M} = [\boldsymbol{\alpha}_2 \ldots \boldsymbol{\alpha}_M]$ and the impact maps. Firstly, the touch down condition of the swing foot at the end of the step

$$z_2(\theta^-, \boldsymbol{\alpha}_M) = 0 \quad (19)$$

is solved for $\theta^-(\boldsymbol{\alpha}_M)$. Subsequently, the configuration before the impact $\mathbf{q}_s^- = \begin{bmatrix} \theta^- \, \boldsymbol{\alpha}_M^T \end{bmatrix}^T$ is mapped onto the one after the impact

$$\mathbf{q}_s^+ = \begin{bmatrix} \theta^+ \\ \boldsymbol{\alpha}_0 \end{bmatrix} = \Psi \left(\mathbf{\Delta}_q \Psi^{-1} \left(\mathbf{q}_s^- \right) \right) \quad (20)$$

using (6), (11) and (17). The impact map (12) for the velocities yields

$$\left(\mathbf{J}_\Psi^+ \right)^{-1} \begin{bmatrix} 1 \\ \frac{M}{\theta^- - \theta^+}(\boldsymbol{\alpha}_1 - \boldsymbol{\alpha}_0) \end{bmatrix} \dot\theta^+$$
$$= \mathbf{\Delta}_{\dot{q}} \left(\mathbf{J}_\Psi^- \right)^{-1} \begin{bmatrix} 1 \\ \frac{M}{\theta^- - \theta^+}(\boldsymbol{\alpha}_M - \boldsymbol{\alpha}_{M-1}) \end{bmatrix} \dot\theta^- \quad (21)$$

with (7), (17) and (18). Since $\dot\theta^+$, $\dot\theta^-$ are unknown, their relation is expressed via the first row of (21)

$$\dot\theta^+ = \mathbf{J}_{\Psi,1}^+ \mathbf{\Delta}_{\dot{q}} \left(\mathbf{J}_\Psi^- \right)^{-1} \underbrace{\begin{bmatrix} 1 \\ \frac{M}{\theta^- - \theta^+}(\boldsymbol{\alpha}_M - \boldsymbol{\alpha}_{M-1}) \end{bmatrix}}_{\mathbf{\Upsilon}} \dot\theta^- \quad (22)$$

and eliminated in the second row which results in

$$\boldsymbol{\alpha}_1 = \boldsymbol{\alpha}_0 + \frac{\theta^- - \theta^+}{M} \left(\mathbf{J}_{\Psi,1}^+ \mathbf{\Upsilon} \right)^{-1} \mathbf{J}_{\Psi,2}^+ \mathbf{\Upsilon} \ . \quad (23)$$

Having thus defined the reference trajectories for the body coordinates, the remaining hybrid zero dynamics must be solved. It is derived from the Lagrangian

$$\mathcal{L}_{HZD}(\theta, \dot\theta) = E_{kin}(\theta, \dot\theta) - E_{pot}(\theta) \quad (24)$$

with the kinetic energy E_{kin} and the potential energy E_{pot}. Applying the method of Lagrange yields the generalized momentum σ and its time derivative

$$\sigma = \frac{\partial}{\partial \dot{\theta}} \mathcal{L}_{HZD} =: \kappa_1^{-1}(\theta) \cdot \dot{\theta} \;, \tag{25}$$

$$\dot{\sigma} = \frac{\mathrm{d}}{\mathrm{d}t}\left(\frac{\partial}{\partial \dot{\theta}}\mathcal{L}_{HZD}\right) = -\frac{\partial}{\partial \theta}\mathcal{L}_{HZD} =: \kappa_2(\theta) \;. \tag{26}$$

The hybrid zero dynamics is

$$\dot{\theta} = \kappa_1(\theta)\,\sigma \;, \tag{27}$$

$$\dot{\sigma} = \kappa_2(\theta) \;. \tag{28}$$

Equations (27) and (28) yield the acceleration

$$\ddot{\theta} = \kappa_1(\theta)\left(\frac{\partial \kappa_1}{\partial \theta}\,\sigma^2 + \kappa_2(\theta)\right) \tag{29}$$

as well as the time free formulation and its solution

$$\frac{\mathrm{d}\sigma}{\mathrm{d}\theta} = \frac{\kappa_2(\theta)}{\kappa_1(\theta)\,\sigma} \;, \tag{30}$$

$$\Rightarrow \quad \frac{1}{2}\sigma^2 = \frac{1}{2}(\sigma^+)^2 + \int_{\theta^+}^{\theta} \frac{\kappa_2(\bar{\theta})}{\kappa_1(\bar{\theta})}\mathrm{d}\bar{\theta} \;. \tag{31}$$

The corresponding time follows from (27)

$$t = \int_{\theta^+}^{\theta} \frac{1}{\kappa_1(\bar{\theta}) \cdot \sigma}\mathrm{d}\bar{\theta} \;. \tag{32}$$

An impact map for the generalized momentum is derived from (22) and (27)

$$\sigma^+ = \frac{\kappa_1(\theta^+)}{\kappa_1(\theta^-)}\left(\mathbf{J}_{\Psi,1}^+ \boldsymbol{\Upsilon}\right)\sigma^- =: \delta \cdot \sigma^- \tag{33}$$

to solve (33) and (31) for

$$\sigma^+ = \delta \cdot \sqrt{\frac{2\int_{\theta^+}^{\theta^-}\left(\kappa_2(\bar{\theta})/\kappa_1(\bar{\theta})\right)\mathrm{d}\bar{\theta}}{1 - \delta^2}} \;. \tag{34}$$

The derived equations allow for the calculation of a periodic gait (Sec. III-B). The gait is stable, if $0 < \delta < 1$ [14].

III. OPTIMIZATION

The robot's cost of transport – the supplied energy divided by the product of distance and weight – is minimized via simultaneous optimization. The objective considers either only one gait with speed $\bar{v}$ or the average cost of transport of several gaits in a speed range $\bar{v} \in [\bar{v}_{min}, \bar{v}_{max}]$. The latter reduces specialization of the design parameters for just one specific speed. The assumptions from Sec. II and the speed $\bar{v}$ are included via constraints.

A. Objective and constraints

The objective and constraints for the simultaneous optimization considering one gait as well as several gaits in a speed range are defined for the model from Sec. II. The optimization parameters are the stiffness k and the independent gait parameters $\boldsymbol{\alpha}_{2M}$ which are merged into the optimization vector $\mathbf{x} = \left[k, \boldsymbol{\alpha}_2^T \ldots \boldsymbol{\alpha}_M^T\right]^T$. The actuators are modeled as geared electric servos with resistance R, torque

constant k_T and gear transmission ratio i_T. The electric power input of the i-th motor is approximated by

$$P_{i,el}(t,\mathbf{x}) = c_{stat}u_{M,i}^2(t,\mathbf{x}) + u_{M,i}(t,\mathbf{x})\dot{q}_{b,i}(t,\mathbf{x}) \tag{35}$$

with the coefficient $c_{stat} = R/(k_T i_T)^2$ [2], [10]. It consists of the motor's heat losses $c_{stat}u_{M,i}^2(t,\mathbf{x})$ and the mechanical work $u_{M,i}(t,\mathbf{x})\dot{q}_{b,i}(t,\mathbf{x})$. With the additional assumption that energy cannot be recuperated when the motors are driven in generator mode, the supplied power is

$$P_i(t,\mathbf{x}) = \max(P_{i,el}(t,\mathbf{x}), 0)$$
$$\approx \frac{1}{2}\left(P_{i,el}(t,\mathbf{x}) + \sqrt{P_{i,el}^2(t,\mathbf{x}) + \varepsilon}\right) \;, \tag{36}$$

where $0 < \varepsilon \ll 1$. The $\max$ function is regularized to comply with the requirement of holomorphicity in Sec. IV-B. The energy efficiency of one gait is quantified by the cost of transport

$$f(\mathbf{x}) = \frac{\sum_{i=1}^{4}\int_0^{t^-} P_i(t,\mathbf{x})\,\mathrm{d}t}{\ell_{Step}(\mathbf{x})\,mg} \;, \tag{37}$$

the supplied energy of all actuators during one step divided by the step length $\ell_{Step} = x_2(\mathbf{q}_s^-)$ and the robot's weight mg.

The assumptions from Sec. II as well as the gait's target speed $\bar{v}$ are formulated as constraints. The target speed is an equality constraint

$$g(\mathbf{x}) = \bar{v} - \frac{\ell_{Step}}{t^-} = 0 \;. \tag{38}$$

The inequality constraints

$$\mathbf{h}(\mathbf{x}) = [h_1(\mathbf{x}) \ldots h_7(\mathbf{x})]^T \leq \mathbf{0} \tag{39}$$

are

$$h_1(\mathbf{x}) = -F_{1,z} \;, \qquad h_2(\mathbf{x}) = -\hat{F}_{2,z} \;, \tag{40}$$

$$h_3(\mathbf{x}) = |F_{1,x}| - \mu_0|F_{1,z}| \;, \quad h_4(\mathbf{x}) = |\hat{F}_{2,x}| - \mu_0|\hat{F}_{2,z}| \;, \tag{41}$$

$$h_5(\mathbf{x}) = -z_2 \;, \tag{42}$$

$$h_6(\mathbf{x}) = -\theta_{K1} \;, \qquad h_7(\mathbf{x}) = -\theta_{K2} \tag{43}$$

and represent unilateral ground contact (40), static friction with coefficient μ_0 (41), no scuffing of swing foot (42) and no hyperextension of the knees (43).

The average cost of transport $\bar{f} = \int_{\bar{v}_{min}}^{\bar{v}_{max}} f(\bar{v})\,\mathrm{d}\bar{v}$ is chosen as objective for the optimization with several gaits. The speed range $\bar{v} \in [\bar{v}_{min}, \bar{v}_{max}]$ is discretized into P equidistant intervals which are evaluated at their midpoints $\bar{v}_p = \bar{v}_{min} + \frac{2p-1}{2P}(\bar{v}_{max} - \bar{v}_{min})$ to approximate the integral by a step function which results in

$$\bar{f}(\bar{\mathbf{x}}) = \frac{1}{P}\sum_{p=1}^{P} f(\mathbf{x}_p) \;. \tag{44}$$

The vector $\bar{\mathbf{x}} = \left[k\,\boldsymbol{\alpha}_{2,1}^T \ldots \boldsymbol{\alpha}_{M,1}^T \ldots \boldsymbol{\alpha}_{2,P}^T \ldots \boldsymbol{\alpha}_{M,P}^T\right]^T$ contains the parameters $\mathbf{x}_p = \left[k\,\boldsymbol{\alpha}_{2,p}^T \ldots \boldsymbol{\alpha}_{M,p}^T\right]^T$ for every gait. Furthermore, (38) – (43) must hold for all gaits, yielding the constraints

$$\bar{\mathbf{g}}(\bar{\mathbf{x}}) = [g(\mathbf{x}_1), \ldots, g(\mathbf{x}_P)]^T \;, \tag{45}$$

$$\bar{\mathbf{h}}(\bar{\mathbf{x}}) = [\mathbf{h}(\mathbf{x}_1), \ldots, \mathbf{h}(\mathbf{x}_P)]^T \;. \tag{46}$$

The objective and constraints of the simultaneous optimization with one gait result from the special case $P = 1$, $\bar{v} = \bar{v}_{min} = \bar{v}_{max}$.

B. Numerical evaluation and implementation

The simultaneous optimization is implemented using the computer algebra system *Maple* and the Software *Matlab*. The implementation in *Maple* and *Matlab* is available as supplementary material, cf. [29]. Equations (1) – (34) are derived as symbolic expressions in *Maple* and exported to *Matlab* functions via automatic code generation. The numerical evaluation is performed in *Matlab* using the SQP algorithm in `fmincon`.

The implementation is presented in detail to allow for the error analysis in Sec. IV. Firstly, the evaluation of (37), (38) and (39) is discussed since $\bar{f}(\bar{\mathbf{x}})$, $\bar{\mathbf{g}}(\bar{\mathbf{x}})$ and $\bar{\mathbf{h}}(\bar{\mathbf{x}})$ are composed of $f(\mathbf{x}_p)$, $g(\mathbf{x}_p)$ and $\mathbf{h}(\mathbf{x}_p)$ ($p \in \{1, \ldots, P\}$) respectively. Subsequently, the gradient approximations and the iterative optimization sequence are presented.

The workflow for the computation of the cost of transport $f(\mathbf{x})$ and constraints $g(\mathbf{x})$, $\mathbf{h}(\mathbf{x})$ for one gait is as follows: Firstly the complete set of gait parameters $\boldsymbol{\alpha}$, θ^+ and θ^- is computed. The SSP is then discretized at N grid points

$$\boldsymbol{\theta} = [\theta_1, \ldots, \theta_N] \,,$$
$$\theta_n = \theta^+ + \frac{n-1}{N-1}\left(\theta^- - \theta^+\right) \,, \quad n \in \{1, \ldots, N\} \quad (47)$$
$$\mathbf{q}_{b,n} = \mathbf{q}_b(\boldsymbol{\alpha}, \theta_n) \quad (48)$$

to approximate the occurring integrals in the further course of the evaluation via quadrature. Subsequently, the first (34), (31) and second integral (32) are approximated via trapezoidal rule T^N at the N grid points. With the solution of the HZD, the velocities (27), (15), accelerations (29), (16) and actuator torques (3), (2) are computed. The cost of transport $f(\mathbf{x})$ is approximated by a third application of the trapezoidal rule. The constraints $\mathbf{g}(\mathbf{x})$ and $\mathbf{h}(\mathbf{x})$ are evaluated for all grid points. Furthermore, the gradients $\partial f / \partial \mathbf{x}$, $\partial g / \partial \mathbf{x}$ and $\partial \mathbf{h} / \partial \mathbf{x}$ are computed via complex step derivative approximation (CSD) [26], [27] of $f(\mathbf{x})$, $\mathbf{g}(\mathbf{x})$ and $\mathbf{h}(\mathbf{x})$. An error analysis for the implementation's numerical approximations is performed in Sec. IV.

Fig. 2 depicts the implementation of the simultaneous optimization

$$\min_{\bar{\mathbf{x}}} \bar{f}(\bar{\mathbf{x}}) \quad \text{subject to} \quad \bar{\mathbf{g}}(\bar{\mathbf{x}}) = \mathbf{0} \,, \quad \bar{\mathbf{h}}(\bar{\mathbf{x}}) \leq \mathbf{0} \,. \quad (49)$$

In the j-th iteration step, the optimization vector $\bar{\mathbf{x}}^j$ is first separated into the parameters $\mathbf{x}_p^j$ for every gait. The cost of transport, the constraints and the respective gradients are then computed for all gaits and subsequently combined into $\bar{f}(\bar{\mathbf{x}})$, $\bar{\mathbf{g}}(\bar{\mathbf{x}})$, $\bar{\mathbf{h}}(\bar{\mathbf{x}})$, $\partial \bar{f} / \partial \bar{\mathbf{x}}$, $\partial \bar{\mathbf{g}} / \partial \bar{\mathbf{x}}$ and $\partial \bar{\mathbf{h}} / \partial \bar{\mathbf{x}}$. Finally, `fmincon` checks the optimality criterion [30] and terminates the iteration with $\bar{\mathbf{x}}^*$ if it holds. If not, $\bar{\mathbf{x}}^{j+1}$ is computed and the iteration continues.

The parameters in Tab. I are used unless stated otherwise. The dimensions and mass distributions resemble an average adult human [31]. $M = 6$ is arbitrarily chosen as in [13]. A
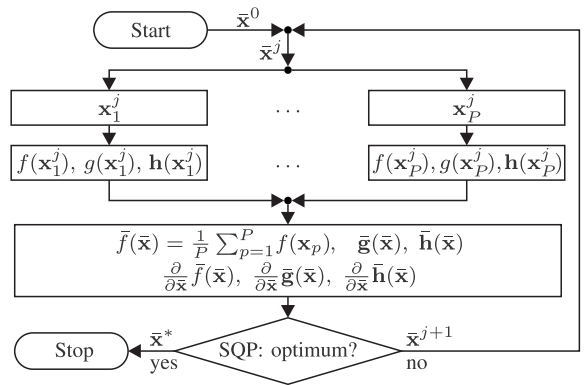

Fig. 2. Algorithm to solve optimization problem (49) for several speed simultaneously.

small value restricts the solution space of possible gaits, a large value increases the number of optimization parameters and thus computation time. The grid size N and the complex step size h_{CSD} are investigated in Sec. IV.

IV. ERROR ANALYSIS

The convergence of the implementation for several gaits with gradient approximations via finite differences (FD) is found to be insufficient which is resolved via bilevel optimization in [1], [2]. Therefore, an error analysis which investigates sources of numerical errors is performed to improve convergence of the presented single-level approach. The analysis focuses on the numerical approximation of the integrals in (34), (31), (32) and (37) in Sec. IV-A as well as the numerical differentiation for the gradient approximations in Sec. IV-B. All investigations are performed for the optimal gaits with speeds $\bar{v}_i \in \{0.3, 0.4 \ldots 2.3\}$ m/s and $k = 0$ Nm/rad unless stated otherwise.

TABLE I

MODEL PARAMETERS

Parameter		Value	Unit
ℓ	total body height	1.80	m
m	total body mass	80.0	kg
m_{HAT}	upper body mass	48.2	kg
m_t	thigh mass	4.56	kg
m_s	shank mass	11.3	kg
ℓ_{HAT}	upper body length	0.533	m
ℓ_t	thigh length	0.446	m
ℓ_s	shank length	0.446	m
r_{HAT}	center of mass position upper body	0.289	m
r_t	center of mass position thigh	0.267	m
r_s	center of mass position shank	0.183	m
J_{HAT}	moment of inertia upper body	3.09	kg m^2
J_t	moment of inertia thigh	0.126	kg m^2
J_s	moment of inertia shank	0.244	kg m^2
g	gravity	9.81	m/s
μ_0	coefficient of static friction	0.6	-
c_{stat}	coefficient of static power	1.81e$-$3	W/ (Nm)^2
M	degree of Bézier polynomials	6	-
N	grid size (SSP)	201	-
P	grid size (speed range)	10	-
h_{CSD}	step size (CSD)	1e$-$100	-

A. Numerical integration

The three consecutive quadratures are considered in the error analysis to validate the code generated by *Maple* and to eliminate error propagation as possible cause of bad convergence. Validation of the generated code is performed via comparison of an estimate for the experimental order of convergence (EOC) to the theoretical order. Deviations indicate errors due to cancellation in the evaluated code. The theoretical model error of the composite trapezoidal rule T^N is of second order [32]. The approximation error of the i-th ($i \in \{1,2,3\}$) integral I_i is estimated via $E_i(T_i^N) = \left|T_i^N - I_i\right| \approx \left|T_i^N - T_i^{5e3}\right|$. The EOC is then computed via

$$q_i \approx \frac{\ln\left(E_i(T_i^{5e2})/E_i(T_i^{5e1})\right)}{\ln\left(50/500\right)} \tag{50}$$

The choice of T_i^{5e3}, T_i^{5e2} and T_i^{5e1} for this estimation is arbitrary. The results in Fig. 3 are in good agreement with the theoretical order $q = 2$. Only three values differ by more than 3%, the greatest deviation being 15% for the third quadrature at $\bar{v} = 1.1$ m/s.

The computation time for one evaluation of the cost of transport, the constraints and the gradients is proportional to the grid size N. The grid $N = 201$ is a good compromise between accuracy and computation time. The absolute and relative error compared to $N = 5e3$ for $\bar{v} = 2.3$ m/s are $7e-5$ and $4e-4$ respectively.

The integrals are built on one another, thus error propagation is regarded via the integrals' conditions [33]

$$\zeta_i = \frac{I_i(|f_i|)}{|I_i(f_i)|} \approx \frac{T_i^N(|f_i|)}{|T_i^N(f_i)|} \ . \tag{51}$$

The second and third integral are of relative condition $\zeta_2 = \zeta_3 = 1$, since the integrands are strictly positive. The relative condition of the first integral is displayed in Fig. 4. ζ_1 increases with decreasing average speed $\bar{v}$ and is at maximum for $\zeta_1 = 23.8$ at $\bar{v} = 0.3$. This means that the achievable precision decreases by less than two digits due to the condition. Therefore, we conclude that the quadratures are not critical for the optimization algorithm.
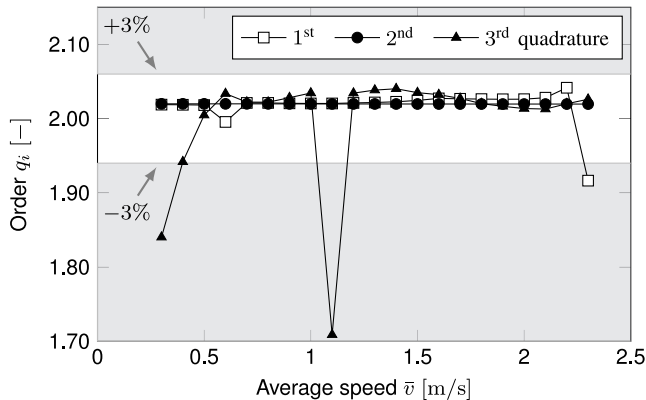
B. Numerical differentiation

The gradients of the objective (44) and constraints (45), (46) have to be approximated since an analytical solution is not available. The accuracy of the gradient approximation might be crucial for convergence of the SQP algorithm because the gradients enter into the evaluation of the optimality conditions as well as the update of the optimization vector. Three numerical methods are considered: finite differences, automatic differentiation [35] and complex step derivative approximation.

Forward (FFD) and central finite differences (CFD) both converge to the exact value for vanishing step size h_{FFD}, h_{CFD}. Due to finite accuracy of $\epsilon \approx e-16$ for floating-point double-precision variables, small step sizes are accompanied by increasing cancellation. The best trade-off between method and cancellation error is $h_{FFD} \approx x_j\sqrt{\epsilon}$ and $h_{CFD} \approx x_j\sqrt[3]{\epsilon}$ respectively [34]. The achievable precision decreases from about $e-16$ to $e-8$ for FFD and $e-11$ for CFD respectively.

Automatic differentiation (AD) is one method to compute derivatives with machine precision. Several toolboxes [36] are available for *Matlab* from which *ADIMAT* [37] was tested due to its free availability and high functionality. However, this implementation increases computation times significantly which is why AD is discarded.

Another method with machine precision is complex step derivative approximation (CSD) [26], [27] which can be implemented analogously to FFD without additional toolboxes. If f is a real function with a real argument and also holomorphic, its CSD is

$$\frac{\partial f(\mathbf{x})}{\partial x_j} = \frac{\text{Im}\{f(\mathbf{x} + ih_{CSD}\mathbf{e}_j)\}}{h_{CSD}} \tag{52}$$

with the j-th unit vector $\mathbf{e}_j$ and step size h_{CSD}. CSD converges second order. Contrary to FD, however, no subtractions are required which means there is no lower limit on step size due to cancellation. $h_{CSD} = 1e-100$ is arbitrarily chosen to compute gradients with machine precision. For $\bar{v} = 2.3$ m/s, Fig. 5 depicts a comparison between FFD, CFD and CSD for $\partial f(\mathbf{x})/\partial x_5$, the entry in the gradient of

Fig. 3. Experimental order of convergence (q_i) for the three quadratures ($i \in \{1,2,3\}$) compared to theoretical order $q = 2$.
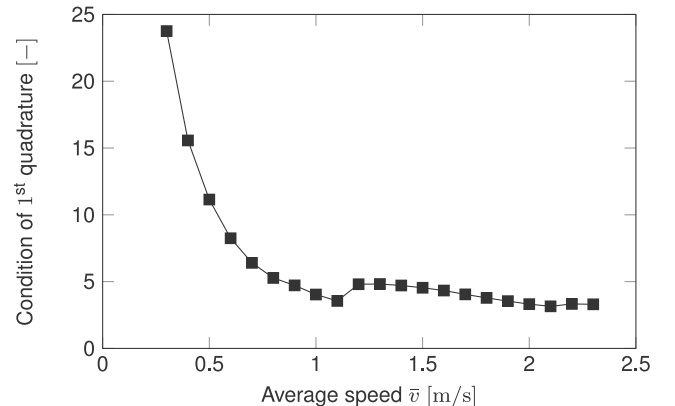

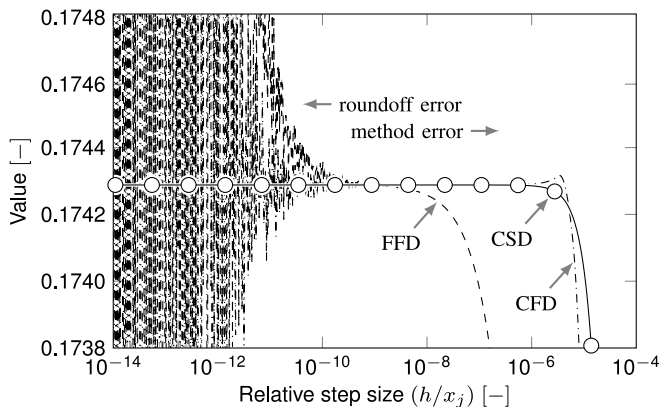Fig. 4. Relative condition of first integral (equations (34), (31)) via (51).

Fig. 5. Forward (FFD) and central finite differences (CFD) compared to complex step derivative approximation (CSD). Labels FFD and CFD at $h_{FFD} = x_j \sqrt{\epsilon}$ and $h_{CFD} = x_j \sqrt[3]{\epsilon}$ respectively.

Fig. 6. Results for simultaneous (sim. opt.) and consecutive optimization (con. opt.) of gait parameters and stiffness for one gait ($\bar{v} = 2.3$ m/s).

the cost of transport with the largest deviations. Large step sizes result in a method error caused by neglect of higher order terms. FFD and CFD suffer from considerable roundoff errors due to cancellation at step sizes below about $1e-9$ resulting in useless approximations. CSD, on the other hand, converge for arbitrarily small step sizes which emphasizes their superiority.

V. RESULTS

The implementation presented for the simultaneous optimization of gait and design parameters is applied to the exemplary model in Sec. II. Two cases are considered: one gait with speed $\bar{v} = 2.3$ m/s and the speed range $\bar{v} \in [0.3, 2.3]$ m/s which is discretized by $P = 10$ gaits. Optimal gaits for $k = 0$ N m/rad are used as initial conditions $\bar{x}^0$ unless stated otherwise. The simultaneous optimization is compared to consecutive optimizations where either the gait is optimized for fixed stiffness, or vice versa. The convergence of the implementation with CSD is compared to FD in terms of achievable accuracy as well as computation times. All computations were performed on a HP Z600 workstation with two Intel Xeon X5650 processors.

The result of the simultaneous optimization considering one gait with $\bar{v} = 2.3$ m/s is displayed in Fig. 6. The convergence to the optimum $k = 886$ N m/rad, $\bar{f}(\bar{x}^*) = 0.0793$ is independent of the derivative approximation (CSD and FD). However, the achievable termination tolerance of the SQP algorithm is only $3e-2$ for FFD compared to $1e-6$ for CSD. The computation times are 45 s for CFD and 120 s for CSD. The longer computation time of CSD is due to the improved accuracy. The energy expenditure $\bar{f}(\bar{x}^*)$ at the optimum is 54.9% lower than the initial value of $\bar{f}(\bar{x}^*) = 0.175$. A consecutive optimization of the stiffness k for the initial gait results in $k = 173$ N m/rad, $\bar{f}(\bar{x}^*_{con}) = 0.156$ (11.3%) which emphasizes the advantage of the presented method.

The results for the speed range $\bar{v} \in [0.3, 2.3]$ m/s are displayed in Fig. 7. The speed range is subdivided into $P = 10$ intervals which are evaluated at their midpoints
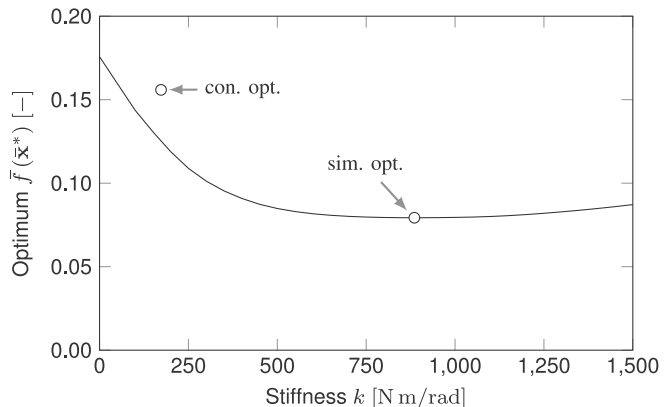
(c.f. Sec. III-A) yielding $\bar{v}_i \in \{0.4, 0.6 \dots 2.2\}$ m/s. The optimization does not converge at all with FD gradient approximation which motivated the error analysis Sec. IV. In contrast, the optimization with CSD converges to the optimum $k = 769$ N m/rad, $\bar{f}(\bar{x}^*) = 0.0312$ which is 60.6% lower than the initial value of $\bar{f}(\bar{x}^0) = 0.0791$. The achievable accuracy is $1e-3$ and the computation time is 175 min. A consecutive optimization of the gaits ($\bar{v}_i \in \{0.4, 0.6 \dots 2.2\}$ m/s) for $k = 886$ N m/rad, the results for one gait, yields $\bar{f}(\bar{x}^*_{con}) = 0.0313$. This is almost identical to the simultaneous optimization because the difference between the stiffnesses and the curvature of the optimal curve in Fig. 7 is small. The optimization of the stiffness for the initial gaits yields a similarly bad result as the consecutive optimization for one gait (not displayed). In general, the quality of a consecutive optimization cannot be predicted a priori whereas the simultaneously optimization converges to the corresponding optimum.

VI. CONCLUSION

A method for simultaneous optimization of gait and design parameters was presented for an exemplary model of a robot
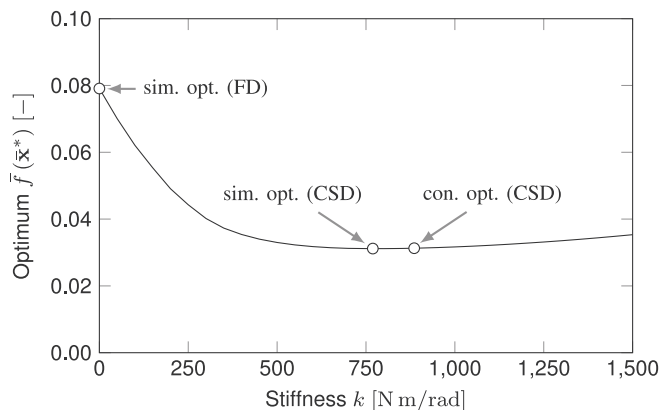

Fig. 7. Results for simultaneous (sim. opt.) and consecutive optimization (con. opt.) of gait parameters and stiffness for ten gaits ($\bar{v}_i \in \{0.4, 0.6 \dots 2.2\}$ m/s). Comparison of finite differences (FD) and complex step derivative approximation (CSD).

with hybrid zero dynamics control. The stiffness of a torsion spring which couples the robot's thighs was optimized with as much as ten gaits simultaneously. An error analysis was performed for the implementation which identified the approximation of gradients as critical for convergence. The implementation of complex step derivative approximation yields good convergence for the considered model.

The simultaneous optimization of stiffness and one gait ($\bar{v} = 2.3$ m/s) results in savings of 55% (computation time: 120 s) compared to a consecutive optimization of firstly gait and subsequently stiffness which yields only 11%. The optimization of the average energy efficiency in the speed range $\bar{v} \in [0.3, 2.3]$ m/s yields as much as 61% (computation time: 175 min) in savings. These examples demonstrate the advantage of the presented method which can easily be transfered to a more complex model or optimize other design parameters (e.g. mass distribution, dimensions). The expansion to a model with feet and the simultaneous optimization of gait and foot shape parameters is intended in future work.

References

[1] F. Bauer, "Optimierung der Energieeffizienz zweibeiniger Roboter durch elastische Kopplungen," Ph.D. dissertation, Karlsruhe Institute of Technology, Karlsruhe, Germany, 2014.

[2] F. Bauer, U. Römer, A. Fidlin, and W. Seemann, "Optimization of energy efficiency of walking bipedal robots by use of elastic couplings in the form of mechanical springs," *Nonlinear Dyn.*, vol. 83, no. 3, pp. 1275–1301, Feb. 2016.

[3] J. E. A. Bertram, "Constrained optimization in human walking: cost minimization and gait plasticity," *J. Exp. Biol.*, vol. 208, no. 6, pp. 979–991, Mar. 2005.

[4] G. Bessonnet, P. Seguin, and P. Sardain, "A parametric optimization approach to walking pattern synthesis," *Int. J. Robot. Res.*, vol. 24, no. 7, pp. 523–536, Jul. 2005.

[5] J. E. Bobrow, F. C. Park, and A. Sideris, "Recent advances on the algorithmic optimization of robot motion," in *Fast Motions in Biomechanics and Robotics*, M. Diehl, and K. Mombaur, Eds., Berlin, Germany: Springer, 2006, pp. 21–41.

[6] P. H. Channon, S. H. Hopkins, and D. T. Pham, "Simulation and optimization of gait for a bipedal robot," *Math. Comput. Model.*, vol. 14, pp. 463–467, 1990.

[7] C. Chevallereau, and Y. Aoustin, "Optimal reference trajectories for walking and running of a biped robot," *Robotica*, vol. 19, no. 05, pp. 557–569, Sep. 2001.

[8] M. L. Felis, and K. Mombaur, "Using optimal control methods to generate human walking motions," ser. Lecture Notes in Computer Science. Berlin, Germany: Springer, 2012, vol. 7660.

[9] K. H. Koch, K. D. Mombaur, and P. Souères, "Studying the Effect of Different Optimization Criteria on Humanoid Walking Motions," ser. Lecture Notes in Computer Science. Berlin, Germany: Springer, 2012, vol. 7628.

[10] U. Römer, A. Fidlin, and W. Seemann, "Investigation of optimal bipedal walking gaits subject to different energy-based objective functions," in *Proc. Appl. Math. Mech.*, vol. 15, no. 1, pp. 69–70, Oct. 2015.

[11] L. Roussel, C. Canudas-de-Wit, and A. Goswami, "Generation of Energy Optimal Complete Gait Cycles for Biped Robots," in *Proc. IEEE Int. Conf. Robotics Automation*, Leuven, Belgium, May 1998, pp. 2036–2041.

[12] M. Scheint, M. Sobotka, and M. Buss, "Compliance in gait synthesis: Effects on energy and gait," in *Proc. IEEE Int. Conf. Humanoid Robots*, Daejeon, Korea, Dec. 2008, pp. 259–264.

[13] E. R. Westervelt, J. W. Grizzle, and D. E. Koditschek, "Hybrid zero dynamics of planar biped walkers," *IEEE Trans. Automat. Control*, vol. 48, no. 1, pp. 42–56, Jan. 2003.

[14] E. R. Westervelt, J. W. Grizzle, C. Chevallereau, J. H. Choi, and B. Morris, *Feedback control of dynamic bipedal robot locomotion*. Boca Raton, FL: CRC, 2007, ch. 3–6.

[15] Y. Xiang, J. S. Arora, and K. Abdel-Malek, "Physics-based modeling and simulation of human walking: a review of optimization-based and other approaches," *Struct. Multidiscip. Optim.*, vol. 42, no. 1, pp. 1–23, Mar. 2010.

[16] K. Mombaur, M. Scheint, and M. Sobotka, "Optimal Control and Design of Bipedal Robots with Compliance," *at-Automatisierungstechnik*, vol. 57, no. 7, pp. 349–359, Jul. 2009.

[17] M. Vukobratović, and B. Borovac, "Zero-moment point - thirty five years of its life," *Int. J. Hum. Robot.*, vol. 1, no. 1, pp. 157–173, Mar. 2004.

[18] J. Pratt, J. Carff, S. Drakunov, and A. Goswami, "Capture point: A step toward humanoid push recovery," in *Proc. IEEE Int. Conf. Humanoid Robots*, Genoa, Italy, Dec. 2006, pp. 200–207.

[19] J. Lack, M. J. Powell, and A. D. Ames, "Planar multi-contact bipedal walking using hybrid zero dynamics," in *Proc. IEEE Int. Conf. Robotics Automation*, Hong Kong, China, Jun. 2014, pp. 2582–2588.

[20] M. Scheint, M. Sobotka, and M. Buss, "Virtual holonomic constraint approach for planar bipedal walking robots extended to double support," in *Proc. IEEE Int. Conf. Decision Control*, Shanghai, China, Dec. 2009, pp. 8180-8185.

[21] C. Chevallereau, G. Abba, Y. Aoustin, F. Plestan, E. Westervelt, C. C. De Wit, and J. Grizzle, "Rabbit: A testbed for advanced control theory," *IEEE Contr. Syst. Mag.*, vol. 23, no. 5, pp. 57–79, Oct. 2003.

[22] T. Yang, E. R. Westervelt, J. P. Schmiedeler, and R. A. Bockbrader, "Design and control of the planar bipedal robot ERNIE," in *Proc. ASME Int. Mechanical Engineering Congress and Exposition*, Seattle, WA, Nov. 2007, pp. 1217–1223.

[23] K. Sreenath, H. W. Park, and J. W. Grizzle, "Design and experimental implementation of a compliant hybrid zero dynamics controller with active force control for running on MABEL," in *Proc. IEEE Int. Conf. Robotics Automation*, St. Paul, MN, May 2012, pp. 51–56.

[24] V. Duindam, and S. Stramigioli, "Optimization of Mass and Stiffness Distribution for Efficient Bipedal Walking," in *Proc. 2005 Int. Symp. Nonlinear Theory and Its Applications*, Bruges, Belgium, Oct. 2005, pp. 481–484.

[25] T. Yang, E. R. Westervelt, and J. P. Schmiedeler, "Using Parallel Joint Compliance to Reduce the Cost of Walking in a Planar Bipedal Robot," in *Proc. ASME Int. Mechanical Engineering Congress and Exposition*, Seattle, WA, Nov. 2007, pp. 1225–1231.

[26] J. N. Lyness, and C. B. Moler, "Numerical differentiation of analytic functions," *SIAM J. Numer. Anal.*, vol. 4, no. 2, pp. 202–210, Jun. 1967.

[27] J. R. R. A. Martins, P. Sturdza, and J. J. Alonso, "The complex-step derivative approximation," *ACM Trans. Math. Software*, vol. 29, no. 3, pp. 245–262, Sep. 2003.

[28] Y. Hurmuzlu, and D. B. Marghitu, "Rigid Body Collisions of Planar Kinematic Chains with Multiple Contact Points," *Int. J. Robot. Res.*, vol. 13, no. 1, pp. 82–92, Feb. 1994.

[29] U. J. Römer, C. Kuhs, M. J. Krause, and A. Fidlin, (2016, Feb.), Supplementary material: Maple and Matlab implementation, Available: http://digbib.ubka.uni-karlsruhe.de/volltexte/beilagen/10/Supplementary_ICRA2016_Roemer_Kuhs_Krause_Fidlin.zip

[30] J. Nocedal, and S. J. Wright, *Numerical Optimization*. New York, NY: Springer, 2006, ch. 18.

[31] P. De Leva, "Adjustments to Zatsiorsky-Seluyanov's segment inertia parameters," *J. Biomech.*, vol. 29, no. 9, pp. 1223–1230, Sep. 1996.

[32] W. Dahmen, and A. Reusken, *Numerik für Ingenieure und Naturwissenschaftler*. Berlin, Germany: Springer, 2008.

[33] R. M. Corless, and N. Fillon, *A Graduate Introduction to Numerical Methods : From the Viewpoint of Backward Error Analysis*. New York, NY: Springer, 2013.

[34] J. E. Dennis, R. B. Schnabel, *Numerical Methods for Unconstrained Optimization and Nonlinear Equations*. Philadelphia, PA: Siam, 1996, pp. 97–106.

[35] A. Griewank, "Evaluating Derivatives: Principles and Techniques of Algorithmic Differentiation," ser. Frontiers in applied mathematics. Philadelphia, PA: Siam, 2000, vol. 19.

[36] M. Bücker, and P. Hovland, (2015, Aug.), AD Tools for MATLAB, [Online], Available: http://www.autodiff.org/?module=Tools&language=MATLAB

[37] C. H. Bischof, H. M. Bücker, B. Lang, A. Rasch, and A. Vehreschild, "Combining Source Transformation and Operator Overloading Techniques to Compute Derivatives for MATLAB Programs," in *Proc. IEEE Int. Workshop Source Code Analysis and Manipulation*, Los Alamitos, CA, Oct. 2002, pp. 65–72.